Chromate-Free Smart Release Corrosion Inhibitive Pigments Containing Cations

P.C.Dodds *

Materials Research Centre, College of Engineering, Swansea University, Bay Campus, Swansea, UK, SA1 8EN.
Advanced Coatings Group, Surface Engineering Department, Tata Steel Research Development and Technology, Sir William Lyons Road, University of Warwick Science Park, Coventry, CV4 7EZ

G. Williams, J. Radcliffe

Materials Research Centre, College of Engineering, Swansea University, Bay Campus,

Crymlyn Burrows, Swansea, UK, SA1 8EN.

e-mail : p.c.dodds@swansea.ac.uk

Abstract

A smart release chrome-free inhibiting system is utilised in an organic coating system to inhibit cathodic disbondment of hot dip galvanised steel. The non-toxic smart release cation system is relatively cheap, easy to process and highly effective. An in-situ scanning Kelvin probe is used to assess the protection offered by the cation containing pigments in a poly-vinyl-butyral model coating. The inhibition of cathodic delamination under the SKP testing conditions exceeds that of hexavalent chromate by the inhibitor system containing magnesium (II) ions.

Introduction

The inclusion of smart-release vehicles within coatings has relieved the constraint of inhibiting species forming part of sparingly soluble salts, to reservoirs of corrosion inhibiting ions that previously would not be considered as part of a primer system. The current chrome free inhibitor Shieldex® is an ion exchanged amorphous silica, that has a reservoir of Ca^{2+} ions, that are released in response to cations in the environment. It is stated by the

manufacturer that in alkaline environments, the amorphous silica will more readily dissolve[1], which is thought to form a protective layer via a hydrated silica gel and metal oxide in the case of iron or possibly zinc silicate anodically inhibiting dissolution of zinc[2]. The inhibitory effects of Shieldex® have been the focus of many investigations [3–6] to assess if it is a contender in replacing hexavalent chromate at protecting iron and zinc substrates, and the mechanisms of action are considered to be; to trap or delay the aggressive ions getting to the metal surface by exchanging them for Ca^{2+} ions, improve cross-linking of the binder, silica and calcium become mobile within the coating and form a protective film on the metal surface[7]. Previous investigations assessing cations as inhibitors have focussed on in-solution cation corrosion inhibitors for zinc[8,9] and the doping of silane pretreatments with rare earth cations to improve the barrier and corrosion properties[10]. Williams et al. investigated the use of cations within the coating to inhibit cathodic disbondment of hot dip galvanised steel (HDG), firstly in naturally occurring Wyoming bentonite clays[11] and later cross-linked sulphonated polystyrene (CSP)[12]. The poor compatibility of bentonite clays and organic coating systems meant that the CSP Dowex® or similar could be viable 'smart' replacements for hexavalent chromate systems.

Cathodic disbondment is the main failure mechanism of organically coated HDG investigated here, and the zinc corrosion cell is simplified into the anodic reaction (Equation 1) and cathodic reaction (Equation 2).

$Zn \rightarrow Zn^{2+} + 2e^-$ **Equation 1**

$O_2 + 2H_2O + 4e^- \rightarrow 4OH^-$ **Equation 2**

The anodic metal dissolution reaction takes place within the defect and the cathodic oxygen reduction reaction takes place under the film at the disbondment front. The elevated pH within the disbonded underfilm environment results in an anodic reaction leading to zincate

formation[13,14], as shown in the pourbaix diagram, where pH above ca. 10.5 leads to bizincate and at higher pH, zincate.

The formation of zincate initiates with the dissolution of the zinc(hydr)oxide surface layer, producing soluble bizincate ($HZnO_2^-$) and zincate (ZnO_2^{2-}) by the following equilibrium reactions,

$$Zn(OH)_{2\,(s)} \rightleftharpoons HZnO_{2\,(aq)}^- + H^+_{(aq)} \quad \textbf{(3)}$$

$$Zn(OH)_{2\,(s)} \rightleftharpoons ZnO_{2\,(aq)}^{2-} + 2H^+_{(aq)} \quad \textbf{(4)}$$

for which the solubility product (K_{sp}) values for the most soluble (amorphous) form of $Zn(OH)_2$ at 25°C are 4.27×10^{-16} M^2 and 1.07×10^{-30} M^3[15].

The mechanism by which certain divalent metal cation (M^{2+}) are principally thought to inhibit cathodic disbondment is through the formation of insoluble metal hydroxides by hydrolysis or partial hydrolysis of M^{2+} by equation 5 and 6:

$$[M(H_2O)_6]^{2+} \rightleftharpoons [M(H_2O)_6OH]^+ + H^+ \qquad \textbf{Equation 5}$$

$$M^{2+} + 2H_2O \rightleftharpoons MOH_2 + 2H^+ \qquad \textbf{Equation 6}$$

This results in the reduction of the under film conductivity and decreases the ion mobility. Others have also argued that in the case of Ca^{2+} cations, the zincate anions formed in the high alkalinity of the cathodic disbondment corrosion cell can also react with the M^{2+} ions to form insoluble $M(OH)_2.2Zn(OH)_2.2H_2O$ or $MZn_2(OH)_6 \cdot 2H_2O$ and thus also reduce underfilm conductivity[11].

To continue previous investigations [11,16], a different matrix system was utilised to store cations, investigating the effectiveness of the cations at inhibiting the corrosion driven cathodic delamination of coated HDG. The matrix used was a crosslinked divinyl benzene

matrix with a sulphonated functional group, with a commercial name of Amberlite®. The form used was the IR120 which has a H^+ counterion making it a strongly acidic ion exchanger. The sulphonate maintains a negative charge and will hold the inhibiting cation in place until the matrix is in contact with a solution containing cations that it will exchange the inhibiting cation for. The use of such ion exchange matrices are common place in effluent discharge for the removal of metal cations such as Ni^{2+}, Zn^{2+}, Ca^{2+} and Mg^{2+} [17,18]. The previous work looking at Dowex® as the exchange matrix, utilised a number of cations to be used as inhibitors and the current research assesses the effect of changing the counterion from Na^+ to H^+ making it a stronger acidic exchanger. The aims of the investigations are:

i) To answer does having H^+ as the counterion affect the exchange efficiency and in turn increase the inhibition when the same cation is used.

ii) To determine the effect of a wider range of potential inhibitors, to include group II cations to identify the relative importance of the formed hydroxide solubility product at inhibiting cathodic delamination.

Experimental Details

Materials Hot dip galvanised (HDG) steel samples consisting of 0.7 mm gauge mild steel coated on both sides with a 20 μm zinc layer containing 0.15 wt.% aluminium were supplied by Tata Steel UK. Amberlite® IR120 (H^+ form), Amberjet® 4200 (Cl^- form), sodium chromate 98%, calcium chloride dihydrate ACS reagent, ≥99%, barium chloride dehydrate ACS reagent, ≥99%, magnesium chloride hexahydrate BioXtra, ≥99.0% and strontium chloride hexahydrate ACS reagent >99%, cerium (III) chloride hexahydrate ≥98.0%, cobalt (II) chloride hexahydrate ACS reagent 98%, polyvinylbutyral-co-vinyl alcohol-co-

vinylacetate (PVB), molecular weight 70,000–100,000, were obtained from the Sigma Aldrich Chemical Company.

Methods

A 0.5M stock solution of each of the metal chloride solutions and sodium chromate solution was made using deionised water, the solutions were added to the resin beads in the ratio of 100ml per 10g of Amberlite® IR120 (cations) or Amberjet® 4200 (chromate) resin beads. Each solution and bead mixture was agitated via stirring for 2 hours, after which the solution was decanted and replaced with fresh stock solution in the same 100ml per original 10g weight ratio. The solutions were stirred for a further 2 hours and again the solution was replaced for fresh stock of 0.5M target metal chloride solution. The beads were left overnight under stirring to ensure maximum exchange had taken place. The beads were filtered using a Buchner filtration system and washed with 500ml of deionised water, to ensure any chloride solution was removed. The beads were dried for 12 hours at 40ºC and then milled using a Retsch planetary ball mill at 350 RPM for 1 hour and sieved through a 20µm mesh. Figure 1 shows the as delivered Amberlite® beads (a), typically 680-820µm in diameter and after processing with the cation exchanged into the matrix (b) with a diameter of <20µm.

The mass of the pigment required for each pigment volume fraction (PVF) was ascertained using:

$$\boldsymbol{Mpig} = \frac{\emptyset \cdot \boldsymbol{M_{pol}} \cdot \boldsymbol{\rho_{pig}}}{(\mathbf{1}-\emptyset) \cdot \boldsymbol{\rho_{pol}}} \qquad \text{Equation 7}$$

Where Mpig is mass of pigment, Mpol is mass of polymer, ρpig is the density of pigment, ρpol is the density of polymer and Ø is the required volume fraction of pigment. The

required mass of the inhibiting pigment for the associated pigment volume fraction was made into an ethanolic slurry, then mixed with the correct amount of PVB, dispersed using a high shear mixer and degassed using a sonicating bath before application to the HDG substrate.

The sample was prepared as described by Strattmann et al[13], where two parallel strips of electrical insulation tape were placed on adjacent sides of the metal coupon, leaving a 15mm strip of bare HDG. A strip of Scotch^{TM} tape was placed over one of the ends of the coupon, covering the insulation tape with the bare metal in the middle. The PVB solution was applied via a drawbar method starting on the Scotch^{TM} tape. Just before the PVB was fully dry, the Scotch^{TM} tape was cut along the boundary between the metal and insulation tape, then lifted and cut to create the lip of the electrolyte well with bare HDG behind in. Non-corrosive silicon was used to provide the electrolyte well walls, holding the lip in place. An electrolyte solution of 0.86 mol dm^{-3} NaCl in deionised water, adjusted to pH 7, was used.

The scanning Kelvin probe (SKP) reference probe was positioned 12mm away from the defect and was scanned towards and perpendicular to the coating-defect boundary. The SKP reference probe was a gold wire with a 125µm diameter, vibrated at 280Hz with an amplitude of 40µm. Scans were taken at 0hrs and every 60 minutes up to 72 hours. A 100µm gap between the reference probe and sample was used, with E_{KP} points measured at 20 per mm. The environmental chamber of the SKP allows a constant humidity of 95% R.H. with the temperature held at 25ºC. Full details of the SKP equipment and calibration have been reported previously[19].

Results and Discussion

Delamination of an un-pigmented Strattmann type cell

The delamination of a PVB coated HDG sample typically initiated within 2 hours of the 0.86 mol dm^{-3} NaCl electrolyte being added to the well. The intact potential of a PVB coated HDG is ca. -400mV vs. SHE, after the calibration has been applied, this is similar to uncoated HDG as seen previously in [12,20]. In Figure 2, the delaminated potential is seen at ca. -650mV vs. SHE, then a second gradual, near linear drop to around -750mV vs. SHE, which represents the link between the delamination front and the defect edge. Between the cathodic activity at the delamination front and the anodic dissolution occurring within the defect, there is an ionic current within the ingressed thin layer of electrolyte beneath the disbonded coating. The ionic current and rate of delamination is determined by the migrational mass transport of Na^+ ions from the defect electrolyte to the delamination front[12]. The sharp inclination between the two is representative of the delamination front, with the point at half way between the intact and delamination potential being X_{del} at the specified time. Each line represents 1 hour, starting (i) 240 minutes, up to 780 minutes where the delamination front has reached 10700µm from the defect. The inset X_{del} vs. time plot is an example of the type of curve for the un-pigmented system and then a strontium chromate inhibited PVB coated HDG system from the point of initiation of delamination ($t-t_i$).

Inhibition by cation loaded Amberlite®

Initial investigations screened different cation exchanged matrix systems at 0.1 pigment volume fraction (PVF) within the PVB model coating. Figure 3 illustrates the different rates of disbondment in the form of an X_{del} vs. time plot, from the point of the delamination cell establishing itself. The diffusion kinetics have been assumed to be parabolic and Kdel values have been calculated from the equation:

$$xdel = kdel(tdel - ti)^{1/2} \qquad \textbf{Equation 8}$$

And are shown in table 1. The cation loaded Amberlite® pigments all inhibit the progression of the delamination front excluding the Na^+ containing matrix, which speeds up the rate of

delamination by ca. 15%. The observation for the Amb-Na^+ pigment demonstrates that the reduction in delamination rate is highly dependent upon cation type, and that stored group I cations, which have soluble hydroxides, have negligible inhibitory properties. The underlying reasons for the slight increase in delamination rate observed for Amb-Na^+ pigment are unclear at present, although one explanation may lie in the ability for in-coating pigments of this type to cause enhanced "short-circuiting" of underfilm ionic species around the PVB/particle interface at high pigment loadings.

The observed rates show that Mg^{2+} ions reacting with the OH^- ions have the highest inhibition followed by the calcium (II) ions reacting with the OH^- ions. The calcium (II) loaded matrix shows no delamination at 1440 minutes (24hrs) after initiation, although a delamination front is seen at 1680 minutes onwards, where the delamination potential is higher than the intact potential, due to the Ca^{2+} ion containing matrix pushing the intact potential to ca. -700mV vs. SHE. This phenomenon has been seen before with cross-linked sulphonated polystyrene matrices loaded with cation inhibitors[16]. The delamination front shows as an increase in potential not the expected potential drop usually seen for delamination potentials. Figure 4 is the time dependant E_{corr} plot for 0.1 PVF of Ca^{2+} pigment addition to PVB on HDG. The Intact potential can be seen at around -700mV vs. SHE and is a direct effect of the Ca^{2+} ions in the matrix. After 1680 minutes the delamination rate is ca. 46 µm min^{-1} up until 1860 minutes, after which the delamination ceased to progress. The decrease in intact potential was also seen for the 0.275 PVF ca^{2+} loaded matrix in PVB, which also had a delamination potential at a higher E_{corr} than the E_{intact}, E_{intact} for the un-pigmented system is ca. -400mV vs. SHE where as the PVB with ca^{2+} pigment showed an E_{intact} of ca. -700mV vs. SHE. The distance travelled by the delamination front in the case of the 0.275 PVF was ca. 2300µm, where as the 0.1 PVF showed ca. 4300µm. There is a decrease in potential from the addition, as well as an inhibiting effect that increases with the

pigment volume fraction of the Ca^{2+} containing pigment. The high level of inhibition shown by Ca^{2+} in Amberlite® shows an improvement on the inhibition offered by the CSP-Ca^{2+} system tested by Williams et al.[12], and this could be attributed to the threefold difference in stated exchange capacity of Amberjet® IR120 (1.8 meq/ml) compared to Dowex® (0.6 meq/ml). The rapid high release of Ca^{2+} ions would lead to a much higher effective concentration of Ca^{2+}, to readily react with any OH^- or negatively charged intermediates of the cathodic oxygen reduction reaction. Theoretically the Amberlite® could hold up to three times the amount of Ca^{2+} within the matrix w/w, resulting in the Amberlite® having three times the inhibiting power over a Dowex®-Ca^{2+} system. It was reported that the inhibitive effectiveness of Ca^{2+} is depends on the total exchange capacity for delivery into the underfilm electrolyte[4,15], to react with the OH^- ions produced by the cathodic oxygen reduction reaction, migrating towards the anode. The concentration of the Ca^{2+} has to be sufficient to form a coherent insoluble precipitate of ($Ca(OH)_2$ or a complex of $[Ca(H_2O)_6OH]^+$) that will block the migration of the Na^+ within the underfilm electrolyte.

The high concentration of Ca^{2+} in the underfilm environment after exchange with Na^+ would form a dynamic equilibrium between the two cations, providing a 2:1 exchange of Na^+ entering the coating versus Ca^{2+} entering the underfilm electrolyte. The driving force behind the Na^+ entering the underfilm environment is reduced, as well as the decrease in the difference between the E_{intact} and $E_{delamination}$, resulting in complementary effects to inhibit the progression of the delamination front.

Inhibition by mg^{2+} containing pigments

The high inhibiting effect of the magnesium ions is can be attributed to the low solubility of the $Mg(OH)_2$ corrosion product that would form between the OH^- of the cathodic oxygen reduction reaction and the Mg^{2+} ions released from the coating matrix into the underfilm environment. The inhibitory effect seen exceeds that of 0.049 PVF $SrCrO_4$ within the same

testing conditions, where strontium chromate containing PVB delaminates to ca. 2850µm within 24 hours (inset Figure 2).

The un-pigmented PVB coated HDG is shown by the parabolic line (0) in Figure 6, in which the rate limiting step in the uninhibited system is the mass transport of Na^+ ions to the delamination front[22]. It shows similar parabolic behaviour for both the 0.02 and 0.05 PVF Amb-Mg^{2+} systems, suggesting that it is still the rate-limiting step, which would agree with the hypothesis that it is insoluble $Mg(OH)_2$ in the underfilm environment, blocking the mass transport of the Na^+ ions from migrating to the delamination front.

Figure 7 is the $(t\text{-}ti)^{1/2}$ vs. Xdel plot for the Amb-Mg^{2+} containing coatings, which shows that the parabolic nature of the un-pigmented system results in a linear fit to the data, however, the 0.02 PVF and 0.05 PVF are not linear, representing a change in delamination kinetics from the un-pigmented system. In the un-pigmented system, the rate-limiting step of the delamination cell is the mass transport of Na^+ ions to the delamination front. The mechanism of inhibition by the Mg^{2+} ions is to react with OH^- from the cathodic oxygen reduction reaction forming an insoluble layer over the substrate surface, hindering the oxygen reduction reaction and is not reliant on the total exchange capacity, creating a blocking of Na^+ ions to the delamination front, but by being present at the cathodic delamination front. This change in kinetics was not obvious from the plots in Figure 6.

The underfilm alkaline environment at ca. -700mV vs. SHE would lead to the formation of zinc oxide, which is n-type semiconductor with a small band gap, which has a room temperature electrical conductivity. Hausbrand et al. previously reported that electron transfer should be affected by semiconductor electrochemistry, which determines the electron concentration at the surface of the semiconductor. The high concentration of electrons at the zinc oxide surface results in a high rate of electron transfer. Magnesium hydroxide has a wide band gap meaning a low electron surface concentration[23], making it a preferred

passive oxide that is an insulator, resulting in low oxygen reduction and metal dissolution in the delaminated area[23]. The zincate and bizincate formed during the anodic processes following the delamination process are soluble at elevated pH and offer little protection under the cathodic front alkaline conditions, where as magnesium hydroxide is stable in alkaline conditions. It is likely that the $Mg(OH)_2$ is very effective at inhibiting cathodic delamination by its wide band gap and stability at high pH[23].

Previous work found that when a magnesium rich zinc oxide was present on the zinc-magnesium substrate, oxygen reduction was inhibited at more negative potentials, and that Mg^{2+}ions within solution were beneficial for zinc corrosion and exposed iron[23]. Kreig et al. also found that $Mg(OH)_2$ reduces oxygen reduction reactivity at the cathodic site, Mg^{2+} cations react more efficiently with OH^- buffering pH[24]. Volvovitch believes that it is not $Mg(OH)_2$ protecting from corrosion, but it is the Mg^{2+} ions promoting and stabilising the formation of simonkolleite[25], this could be the mechanism of inhibition if Mg^{2+} ions were released into the defect, but simonkolleite would not form in the underfilm environment due to the prevention of ingress of chloride ions. An agreed mechanism of protection is the buffering of pH at around 10.2 by the formation of $Mg(OH)_2$[25,26], a stable hydroxide at high pH, blocking electron transfer and decreasing the availability of O_2 at the cathodic site. Similar effects are seen by the insoluble precipitates of cerium (III) ions hindering the oxygen reduction reaction[27].

Effect of the pigment volume fraction of the Mg^{2+} and Ca^{2+} pigments on K_{del} and E_{intact}

Figure 8 shows the decrease in K_{del} with increased PVF of both exchange pigments loaded with $Ca^{2+}$and Mg^{2+} ions. At the lower PVF for the Ca^{2+} containing systems, the 0.05 PVF resulting K_{del} does not decrease significantly from the un-pigmented system, this is likely to be an insufficient concentration of Ca^{2+} within the underfilm electrolyte to be an effective

inhibitor. The rapid drop for the 0.1 PVF Ca^{2+} K_{del} shows that at this level there is sufficient exchange of the Na^{+} and Ca^{2+} to give an effective concentration of Ca^{2+} in the underfilm electrolyte to form calcium zincate. The Mg^{2+} containing system shows a systematic decrease in the K_{del} with respect to PVF, and at 0.1 and 0.2 PVF the high level of inhibition is evident with a K_{del} of 0. The efficiency of the system is thought to be due to the highly insoluble precipitate formed as well as the decrease in E_{intact} with respect to PVF that is observed for both systems. The addition of the cation containing pigment decreases the intact potential of the coating to near the un-pigmented PVB delaminated potential. When assessing the effects of the Ca^{2+} and Mg^{2+} containing pigments, the decrease in the intact potential decreases the driving force of the delamination cell by having a reduced potential difference. Figure 9 shows that the higher the addition of the inhibiting pigment, the more negative E_{intact} becomes at a minimum of ca. -700mV vs. SHE for the highest loading of both pigments. The depression of E_{intact} has been observed previously [11,12], and is proposed to be an effect of the in-coating cations on the inhibition of underfilm cathodic oxygen reduction. The change in K_{del} follows the trend for the lowering of E_{intact} of the coated samples with increased pigment volume fraction and cannot be ruled out as a factor of the inhibiting effect of the pigments.

Group *II cation inhibition*

The insolubility of the hydroxides formed are thought to be the main inhibiting effect of the released metal cations into the underfilm electrolyte, if the K_{sp} is considered for the hydroxides, the K_{sp} for $Mg(OH)_2$ is ca. 2×10^{-13} M^3 and for $Ca(OH)_2$ it is 5×10^{-6} M^3. The lower solubility of the $Mg(OH)_2$ could explain why it is superior at inhibiting the cathodic delamination of the PVB on HDG. It is well documented that the solubility of the hydroxides of the group two metals decreases as you move down the group. Ba^{2+}

ions and Sr^{2+} ions were also incorporated into the Amberlite®, to test the efficiency of the ions at inhibiting cathodic delamination. Figure 10 represents the delamination distance versus time from initiation of the group II ions and un-pigmented PVB. The magnesium and calcium containing pigments show no delamination over the 24 hour period, where as both the strontium and barium containing pigments both delaminate with limited inhibition of cathodic delamination when compared to the uninhibited system. The hydroxides of calcium and magnesium are more insoluble than the strontium and barium hydroxides, which have a K_{sp} of ca. $1.5 \times 10^{-4}\ M^3$ and ca. $5 \times 10^{-3} M^3$, respectfully. The E_{intact} of the Ba^{2+} and Sr^{2+} containing coatings is depressed at the same level as the Mg^{2+} and Ca^{2+} containing coatings, ca. -600-650mV vs. SHE, so this is not a controlling factor for the inhibition of the cathodic delamination of PVB on HDG, although it does contribute to the driving forces of the cell. From the results, it suggests that the high inhibition by the magnesium (II) containing pigment is due to the insolubility of the $Mg(OH)_2$ formed from the products of the cathodic oxygen reduction reaction at the cathodic front, which is represented in the schematic in Figure 10.

However, given the relatively high calcium hydroxide K_{sp} value of $5 \times 10^{-6}\ M^3$, it is more difficult to argue that underfilm precitation of $Ca(OH)_2$ solely accounts for the significant degree of inhibition afforded by the in-coating Ca^{2+}-Amb pigment. If the pH of the underfilm electrolyte is estimated to be pH 11, then precipitation will only occur when the underfilm Ca^{2+} concentration exceeds a highly unlikely 5 M threshold. To investigate the possible role of ambient CO_2 and the potential formation of calcium carbonate in the alkaline underfilm electrolyte as a means of promoting underfilm inhibition, additional experiments on PVB coated HDG containing Amb-Ca^{2+} at a pigment volume fraction of 0.1 were carried out, both in the presence and absence of

carbon dioxide. In the first experiment, a continuous flow of synthetic air at 95% RH was introduced as a continuous flow into the SKP environmental chamber over a 24h period and the delamination kinetics were measured by in-situ SKP E_{corr} mapping. The delamination rate actually decreased by ca 30% compared to the case where static lab air at 95% RH, containing a nominal 0.03% v/v CO_2 concentration. In a separate experiment, an environment consisting of synthetic air at 95% RH containing CO_2 at a 0.1 v/v concentration was maintained in the SKP chamber. For this experiment, a delamination rate was obtained which was very similar to the control carried out in static lab air at the same RH. Both observations are not consistent with the argument that inhibition is principally due to CO_2 permeating through the PVB coating, forming underfilm carbonate anions and precipitating insoluble calcium carbonate in the delaminated zone. Although these observations may not rule out an effect of CO_2 over a longer timescale, over the 24h duration of the experiments described here, it appears that CO_2 plays only a minor role in the underfilm inhibition mechanism of in-coating Ca^{2+} cations.

These observations therefore beg the question as to why exactly the in-coating Ca^{2+} inhibits the cathodic disbondment process so effectively. It has been proposed elsewhere [11], that the underfilm formation of solid calcium zincate salts may account for the significant decrease rate of cathodic disbondment in the presence of in-coating Ca^{2+} inhibitor. Although the equilibrium constants given previously for equations 3 and 4 predict that the zincate concentration [ZnO_2^{2-}] will be low at moderate alkalinity (e.g. ca 10^{-6} M at pH12), nevertheless, it may be sufficient to allow precipitation of solid calcium zincate providing the underfilm Ca^{2+} concentration is high enough for the K_{sp} value to be exceeded (pK = 44.6)[21].

Conclusions

A new smart release inhibiting pigment was utilised in a PVB coating to protect the coated HDG from cathodic disbondment. It was shown that changing the counter ion of the sulphonate group in the organic matrix from Na^+ to H^+ increased the inhibitive performance, when Ca^{2+} ions were utilised, showing the higher inhibitive effect when the Amberlite® matrix is used instead of Dowex® From the screening tests, Mg^{2+} and Ca^{2+} containing pigments were identified as high performing inhibiting pigments. The 0.1 and 0.2 PVF Mg^{2+}pigments showed no sign of delamination under the SKP testing conditions and the high level of inhibition was attributed to the highly insoluble precipitate of $Mg(OH)_2$. The analysis of the different pigment volume fractions of Mg^{2+} containing pigments in PVB showed that at the 0.02 PVF and 0.05 PVF loadings, the rate limiting step had changed from the migrational mass transport of Na^+ ions. The change in the rate limiting step leans towards the $Mg(OH)_2$ hindering oxygen availability and electron transfer processes at the cathodic front. From the systematic testing of Group II cations, it was shown that the solubility of the hydroxide is an important factor for the inhibition of cathodic disbondment of PVB coated HDG.

Acknowledgements

The authors would like to thank the European Social Fund (ESF) and Tata Steel UK for financial support of this work, with special thanks to Dr. Jon Elvins.

Figure Legends

Figure 1. Amberlite® IR120 Resin Beads in As Delivered Form (a) and after processing with the addition of inhibiting cation (b).

Figure 2. E_{corr} vs. distance for un-pigmented PVB on HDG, (i) is 240 minutes after addition of 0.86 mol dm^{-3} electrolyte to the defect and every line is 60 minutes up until (ii) 780 minutes. Inset is a typical X_{del} vs. time plot for an un-pigmented PVB system and a 0.049PVF addition of strontium chromate to the PVB on a HDG substrate (Inset data from [28]).

Figure 3. X_{del} vs. $(t-t_i)$ for the different inhibitors added to the matrices. All additions of the pigments were made at 0.1 PVF to PVB on HDG.

Figure 4. Time dependant E_{corr} versus X_{del} profile for 0.1 PVF addition of Ca^{2+} containing pigment. (i) 1680 minutes (ii)1740 minutes (iii) 1800 minutes (iv) 1860 minutes.

Figure 5. Time dependant E_{corr} versus X_{del} profiles for Mg^{2+} containing pigments in a PVB coating on HDG at 0.05 PVF (a) and 0.2 PVF (b). (a) (i) is 420 minutes, then every 3 hours up until 2220 minutes (a) (ii). (b) represents the time dependant plots up to 2220 minutes.

Figure 6. Plot of delamination distance (x_{del}) vs. $(t-t_i)$ for different pigment volume fractions (0, 0.02, 0.05, 0.1, 0.2) of the Mg^{2+} containing pigment to PVB.

Figure 7. . Plot of delamination distance (x_{del}) vs. $(t-t_i)^{1/2}$ for different pigment volume fractions (0, 0.02, 0.05, 0.1, 0.2) of the Mg^{2+} containing pigment to PVB.

Figure 8. Plot of initial K_{del} vs. ϕ_{pt} for (i) Mg^{2+} and (ii) Ca^{2+} containing pigments incorporated into the PVB coating.

Figure 9. Plot of E_{intact} (mV vs. SHE) versus ϕ_{pt} of (i) Mg^{2+} and (ii) Ca^{2+} containing pigments incorporated into the PVB coating.

Figure 10 Plot of delamination distance (x_{del}) vs. $(t-t_i)$ for PVB coated HDG (i) uninhibited and 0.1 PVF additions of pigments loaded with (ii) Ba^{2+} (iii) Sr^{2+} (iv) Mg^{2+} and (v) Ca^{2+} ions.

Figure 11 Schematic representation of the inhibition of corrosion-driven cathodic disbondment on galvanised steel by in-coating Mg^{2+} containing pigments.

TABLE 1. Values for parabolic rate constant and change from baseline parabolic rate constant for different inhibitors in the Amberlite® added at 0.1 PVF to PVB

Inhibitor in Matrix	**K_{del} ($\mu m\ min^{-1}$)**	**ΔK_{del} (%)**
No Inhibitor	594	0
Na^{+}	685	15
Zn^{2+}	171	-71
Ce^{3+}	132	-77
Co^{2+}	101	-82
CrO_4^{2-}	39	-93
Ca^{2+}	46 (after 1680 mins)	-92
Mg^{2+}	0	-100

References

[1] G.B. Alexander, W.M. Heston, R.K. Iler, The Solubility of Amorphous Silica in Water, J. Phys. Chem. 58 (1954) 453–455.

[2] K. Aramaki, The inhibition effects of chromate-free, anion inhibitors on corrosion of zinc in aerated 0.5 M NaCl, Corros. Sci. 43 (2001) 591–604.

[3] R.. Howard, I.. Zin, J.. Scantlebury, S.. Lyon, Inhibition of cut edge corrosion of coil-coated architectural cladding, Prog. Org. Coatings. 37 (1999) 83–90.

[4] A. Amirudin, C. Barreau, R. Hellouin, D. Thierry, Evaluation of anti-corrosive pigments by pigment extract studies, atmospheric exposure and electrochemical impedance spectroscopy, Prog. Org. Coatings. 25 (1995) 339–355.

[5] F. Deflorian, I. Felhosi, S. Rossi, L. Fedrizzi, P.L. Bonora, Performance of primers containing polyphosphate-based ion-exchange pigments for the protection of galvanised steel, in: Macromol. Symp., 2002: pp. 87–96.

[6] N. Granizo, J.M. Vega, I. Díaz, B. Chico, D. de la Fuente, M. Morcillo, Paint systems formulated with ion-exchange pigments applied on carbon steel: Effect of surface preparation, Prog. Org. Coatings. 70 (2011) 394–400.

[7] L.W. Vasconcelos, I.C.P. Margarit, O.R. Mattos, F.L. Fragata, A.S.B. Sombra, Inhibitory properties of calcium exchanged silica epoxy paintings, Corros. Sci. 43 (2001) 2291–2303.

[8] K. Aramaki, The inhibition effects of cation inhibitors on corrosion of zinc in aerated 0.5 M NaCl, Corros. Sci. 43 (2001) 1573–1588.

[9] H. Leidheiser, Cobalt and Nickel Cations as Corrosion Inhibitors for Galvanized Steel, J. Electrochem. Soc. 128 (1981) 242.

[10] M.F. Montemor, W. Trabelsi, M. Zheludevich, M.G.S. Ferreira, Modification of bis-silane solutions with rare-earth cations for improved corrosion protection of galvanized steel substrates, Prog. Org. Coatings. 57 (2006) 67–77.

[11] G. Williams, H.N. McMurray, M.J. Loveridge, Inhibition of corrosion-driven organic coating disbondment on galvanised steel by smart release group II and Zn(II)-exchanged bentonite pigments, Electrochim. Acta. 55 (2010) 1740–1748.

[12] G. Williams, S. Geary, H.N. McMurray, Smart release corrosion inhibitor pigments based on organic ion-exchange resins, Corros. Sci. 57 (2012) 139–147. 39

[13] W. Fürbeth, M. Stratmann, The delamination of polymeric coatings from electrogalvanised steel – a mechanistic approach., Corros. Sci. 43 (2001) 207–227.

[14] W. Fürbeth, M. Stratmann, Scanning Kelvinprobe investigations on the delamination of polymeric coatings from metallic surfaces, Prog. Org. Coatings. 39 (2000) 23–29.

[15] N. DE Zouboy, M. Pourbaix, Atlas of Electrochemical Equilibria in Aqueous Solutions, Pergamon Press, 1966.

[16] G. Williams, S. Geary, H.N. McMurray, Smart release corrosion inhibitor pigments based on organic ion-exchange resins, Corros. Sci. 57 (2012) 139–147. doi:10.1016/j.corsci.2011.12.024.

[17] Z. Yu, T. Qi, J. Qu, L. Wang, J. Chu, Removal of Ca(II) and Mg(II) from potassium chromate solution on Amberlite IRC 748 synthetic resin by ion exchange., J. Hazard. Mater. 167 (2009) 406–12.

[18] P.E. Franco, M.T. Veit, C.E. Borba, G. da C. Gonçalves, M.R. Fagundes-Klen, R. Bergamasco, et al., Nickel(II) and zinc(II) removal using Amberlite IR-120 resin: Ion exchange equilibrium and kinetics, Chem. Eng. J. 221 (2013) 426–435.

[19] G. Williams, A. Gabriel, A. Cook, H.N. McMurray, Dopant Effects in Polyaniline Inhibition of Corrosion-Driven Organic Coating Cathodic Delamination on Iron, J. Electrochem. Soc. 153 (2006) B425.

[20] I. Mabbett, J. Elvins, C. Gowenlock, C. Glover, P. Jones, G. Williams, et al., Addition of carbon black NIR absorber to galvanised steel primer systems: Influence on NIR cure of polyester melamine topcoats and corrosion protection characteristics, Prog. Org. Coatings. 77 (2014) 494–501.

[21] F. Ziegler, C.A. Johnson, The solubility of calcium zincate (CaZn2(OH)6·2H2O), Cem. Concr. Res. 31 (2001) 1327–1332.

[22] G. Williams, H.N. McMurray, Chromate Inhibition of Corrosion-Driven Organic Coating Delamination Studied Using a Scanning Kelvin Probe Technique, J. Electrochem. Soc. 148 (2001) B377.

[23] R. Hausbrand, M. Stratmann, M. Rohwerder, Corrosion of zinc–magnesium coatings: Mechanism of paint delamination, Corros. Sci. 51 (2009) 2107–2114.

[24] R. Krieg, A. Vimalanandan, M. Rohwerder, Corrosion of Zinc and Zn-Mg Alloys with Varying Microstructures and Magnesium Contents, J. Electrochem. Soc. 161 (2014) C156–C161.

[25] P. Volovitch, C. Allely, K. Ogle, Understanding corrosion via corrosion product characterization: I. Case study of the role of Mg alloying in Zn–Mg coating on steel, Corros. Sci. 51 (2009) 1251–1262.

[26] T. Prosek, D. Persson, J. Stoulil, D. Thierry, Composition of corrosion products formed on Zn–Mg, Zn–Al and Zn–Al–Mg coatings in model atmospheric conditions, Corros. Sci. 86 (2014) 231–238.

[27] H. Wang, R. Akid, Encapsulated cerium nitrate inhibitors to provide high-performance anti-corrosion sol–gel coatings on mild steel, Corros. Sci. 50 (2008) 1142–1148.

[28] G. Williams, H.N. McMurray, Chromate Inhibition of Corrosion-Driven Organic Coating Delamination Studied Using a Scanning Kelvin Probe Technique, J. Electrochem. Soc. 148 (2001)

Figure 1

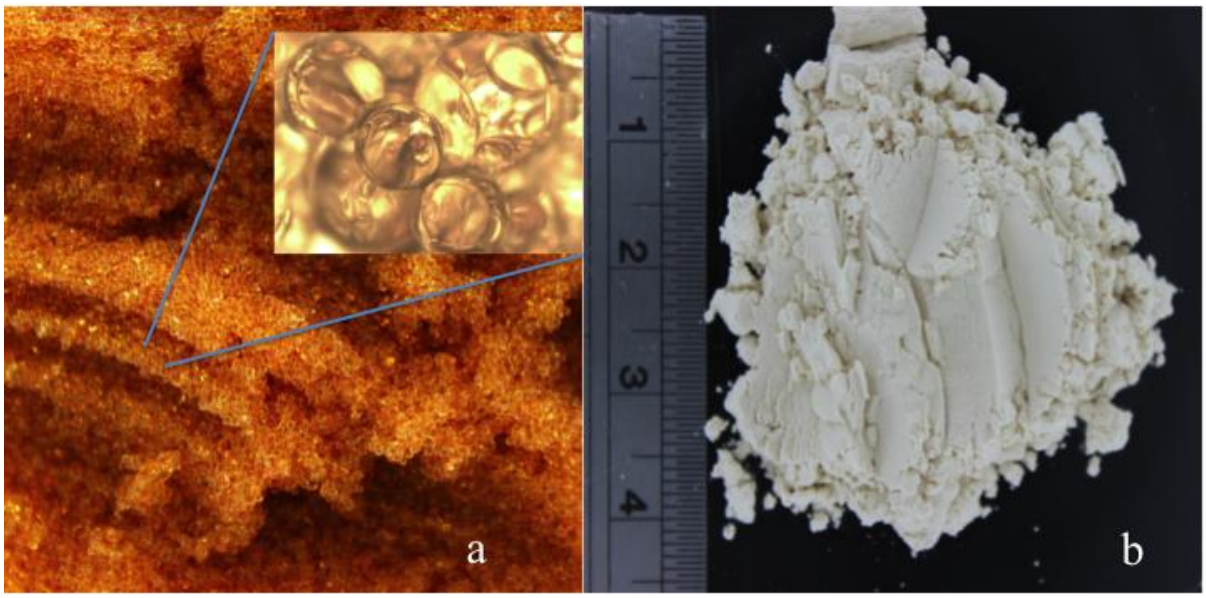

Figure 2

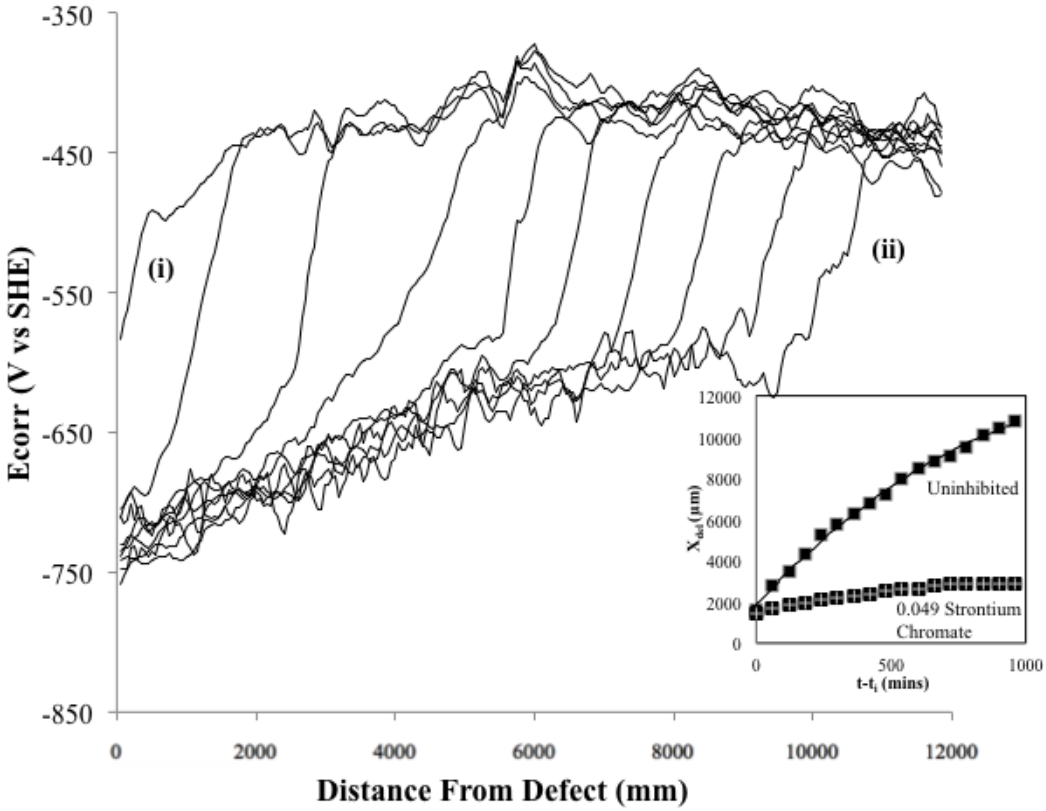
-350
-450
-550
-650
-750
-850
Ecorr (V vs SHE)
(i)
(ii)
0
2000
4000
6000
8000
10000
12000
Distance From Defect (mm)
12000
10000
8000
6000
4000
2000
0
X_{def} (µm)
Uninhibited
0.049 Strontium Chromate
0
500
1000
t-t_i (mins)

Figure 3

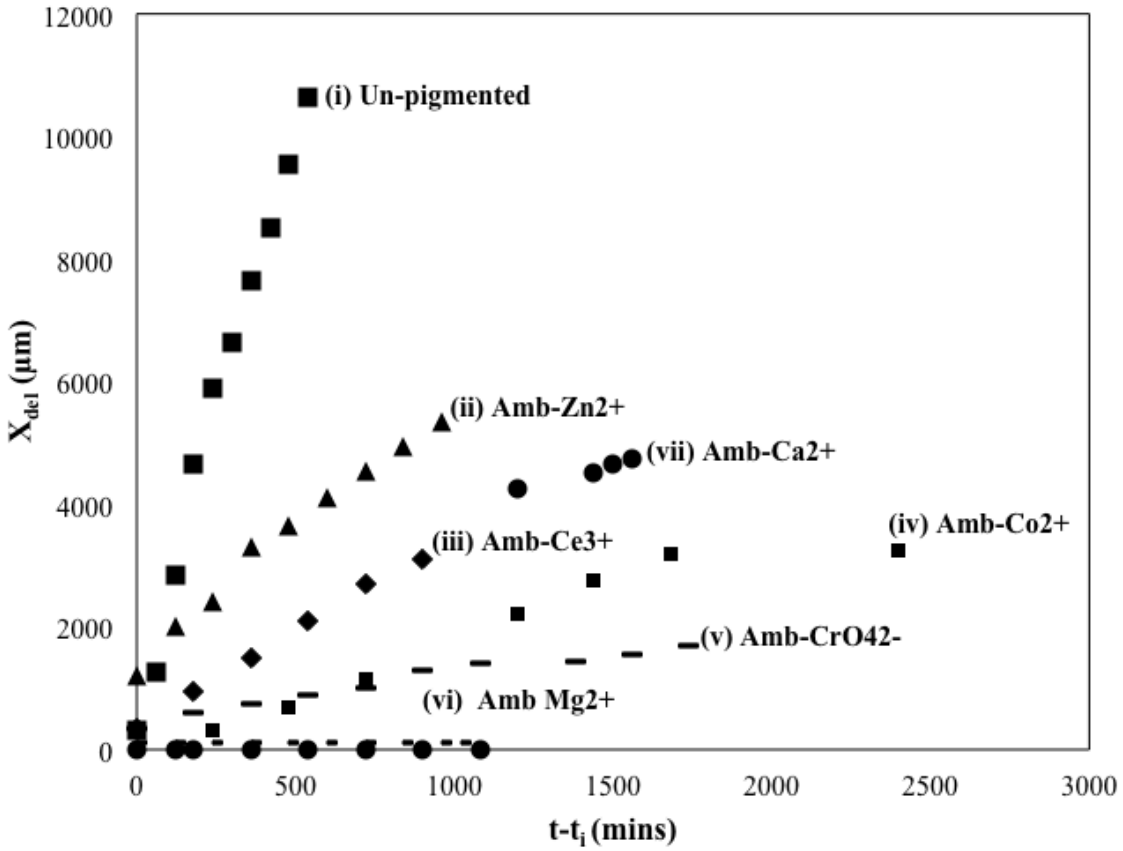
12000
10000
8000
6000
4000
2000
0
X_{del} (µm)
0
500
1000
1500
2000
2500
3000
t-t_i (mins)
(i) Un-pigmented
(ii) Amb-Zn2+
(vii) Amb-Ca2+
(iii) Amb-Ce3+
(iv) Amb-Co2+
(v) Amb-CrO42-
(vi) Amb Mg2+

Figure 4

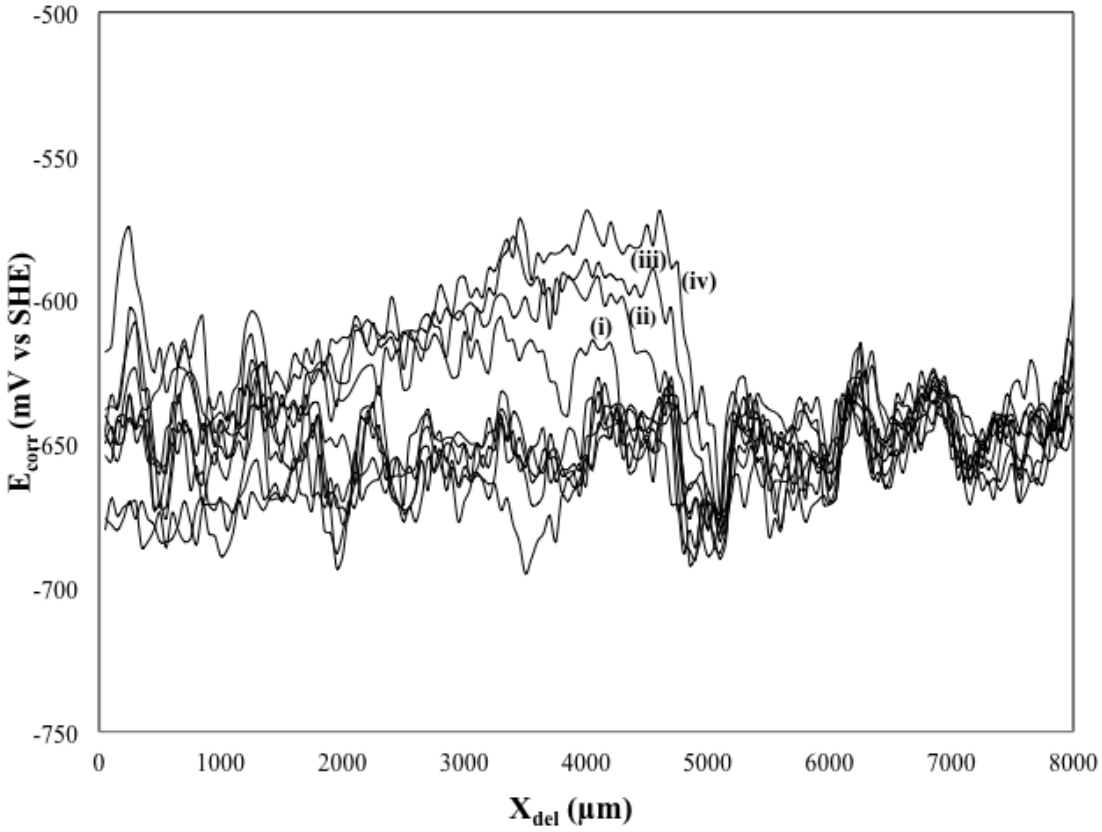
-500
-550
-600
-650
-700
-750
E_{corr} (mV vs SHE)
0
1000
2000
3000
4000
5000
6000
7000
8000
X_{del} (µm)
(i)
(ii)
(iii)
(iv)

Figure 5

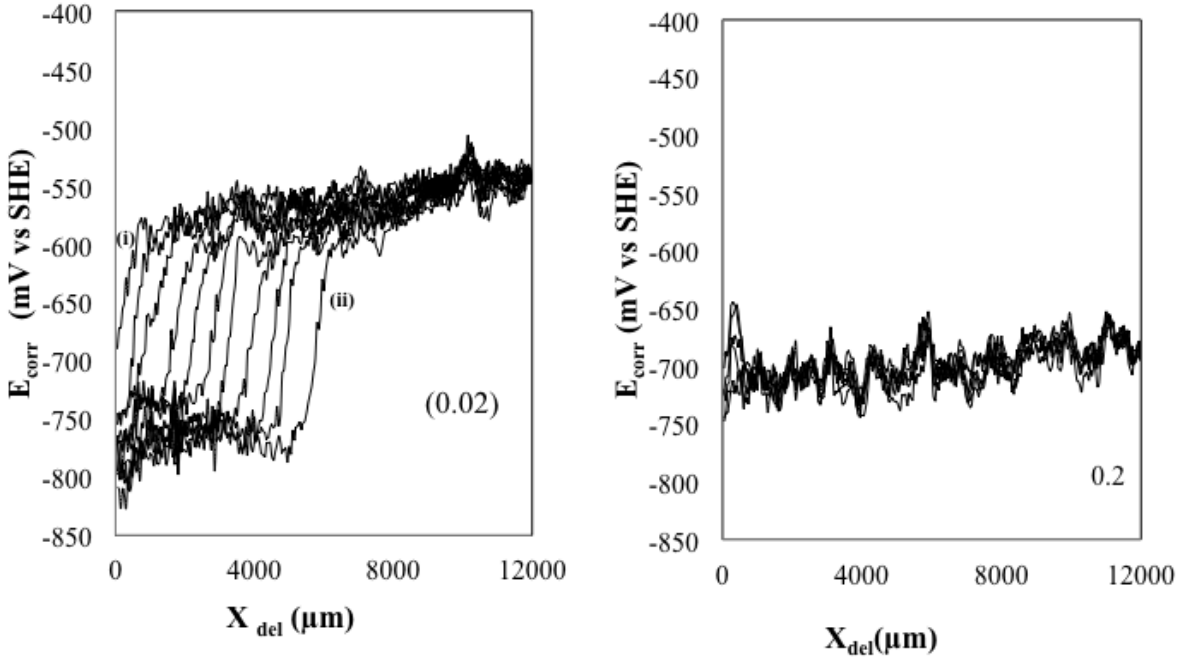

Figure 6

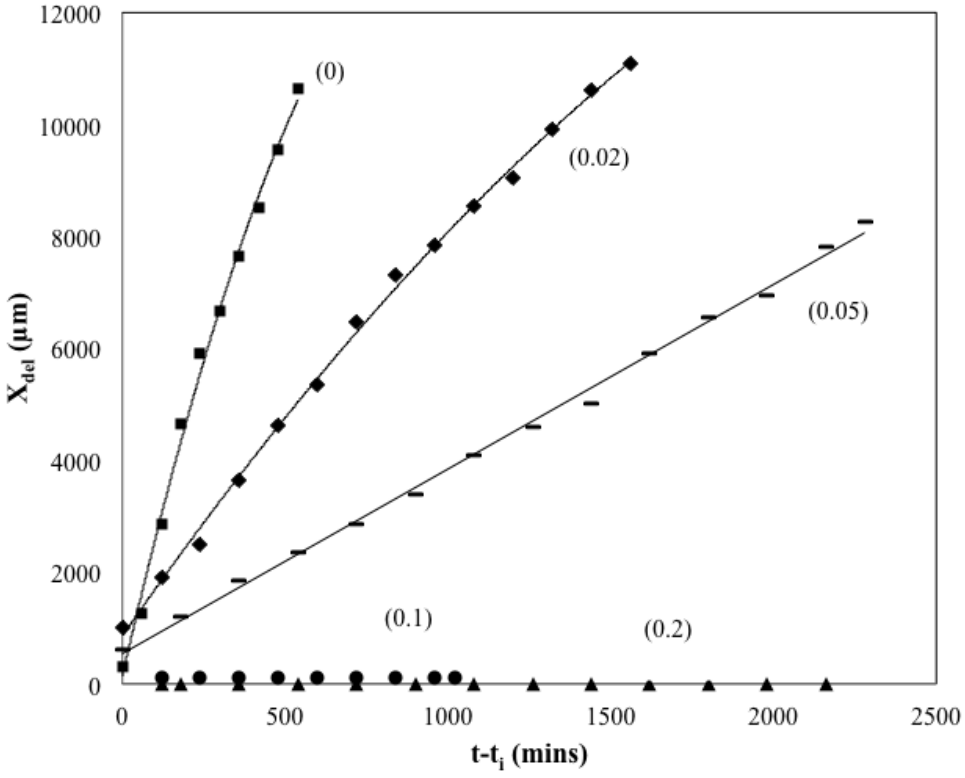

Figure 7

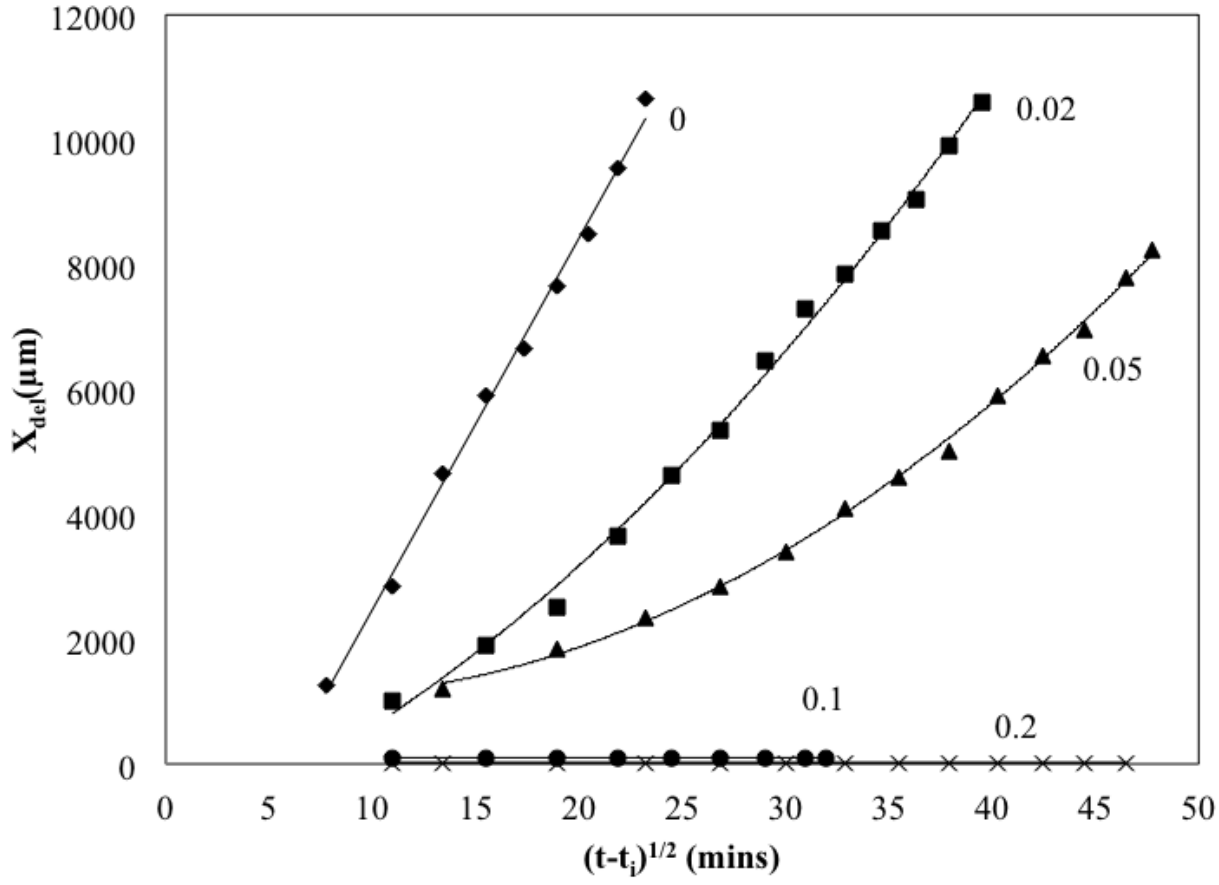
12000
10000
8000
6000
4000
2000
0
0
5
10
15
20
25
30
35
40
45
50
X_{del}(µm)
$(t-t_i)^{1/2}$ (mins)
0
0.02
0.05
0.1
0.2

Figure 8

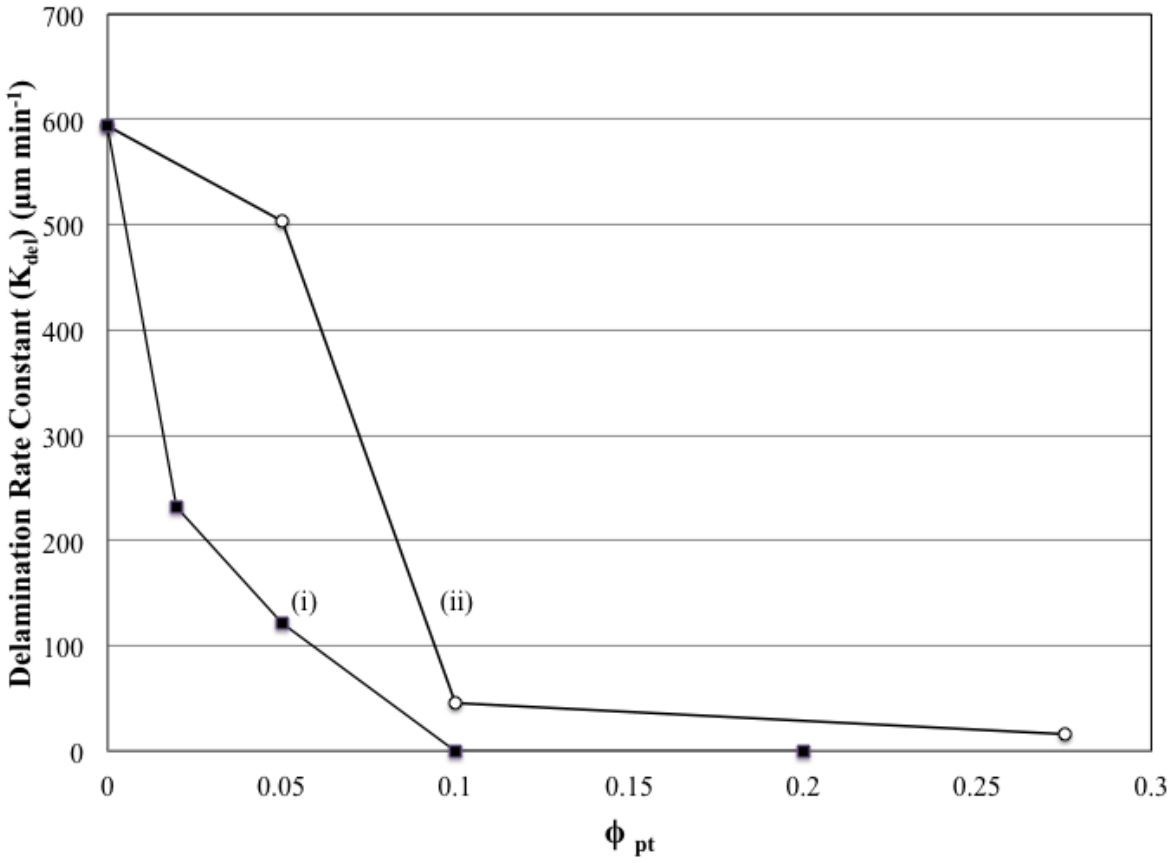
700
600
500
400
300
200
100
0
0
0.05
0.1
0.15
0.2
0.25
0.3
Delamination Rate Constant (K_{del}) (μm min^{-1})
ϕ_{pt}
(i)
(ii)

Figure 9

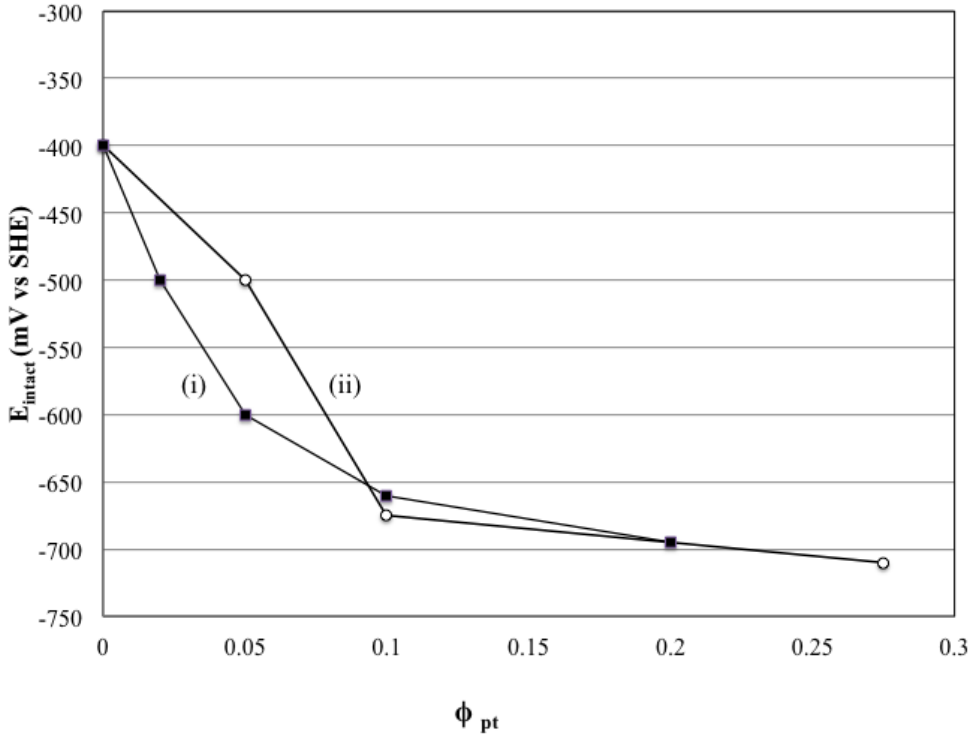

Figure 10

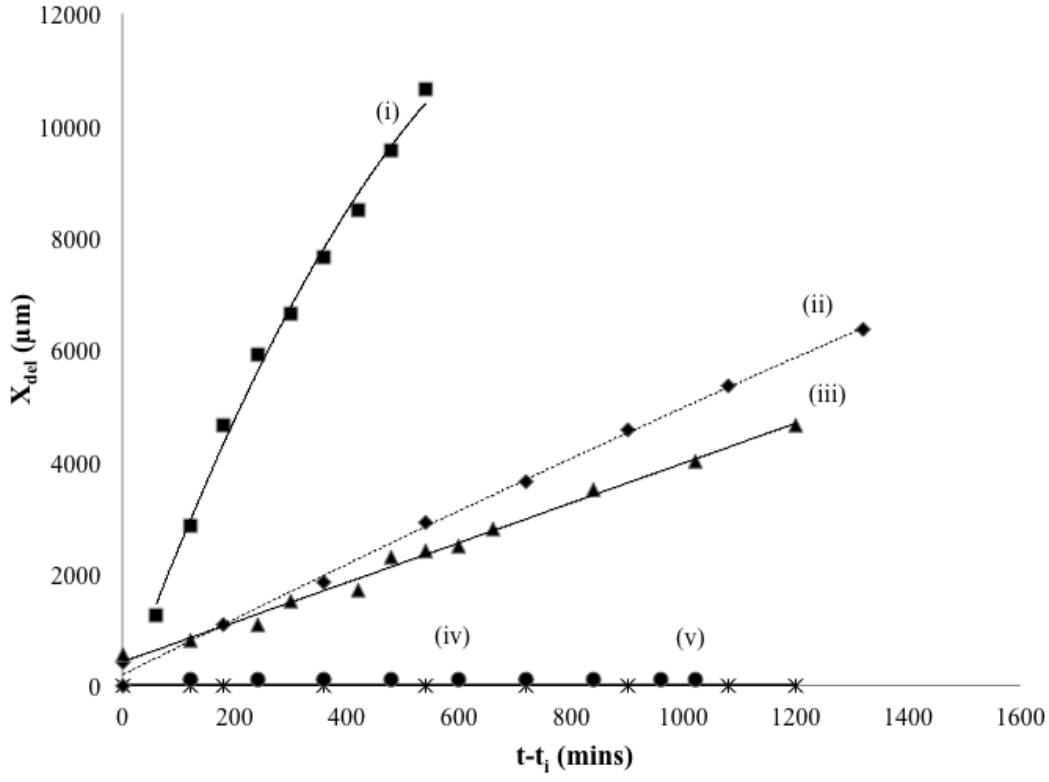

Figure 11